The EMBO Journal (2007) 26, 2966–2980 | © 2007 European Molecular Biology Organization | All Rights Reserved 0261-4189/07
www.embojournal.org

THE EMBO JOURNAL

Distinct IFT mechanisms contribute to the generation of ciliary structural diversity in *C. elegans*

Saikat Mukhopadhyay[1], Yun Lu[2], Hongmin Qin[3,4], Anne Lanjuin[1,5], Shai Shaham[2] and Piali Sengupta[1,*]

[1]Department of Biology and National Center for Behavioral Genomics, Brandeis University, Waltham, MA, USA, [2]Laboratory of Developmental Genetics, The Rockefeller University, New York, NY, USA and [3]Department of Molecular, Cellular and Developmental Biology, Yale University, New Haven, CT, USA

Individual cell types can elaborate morphologically diverse cilia. Cilia are assembled via intraflagellar transport (IFT) of ciliary precursors; however, the mechanisms that generate ciliary diversity are unknown. Here, we examine IFT in the structurally distinct cilia of the ASH/ASI and the AWB chemosensory neurons in *Caenorhabditis elegans*, enabling us to compare IFT in specific cilia types. We show that unlike in the ASH/ASI cilia, the OSM-3 kinesin moves independently of the kinesin-II motor in the AWB cilia. Although OSM-3 is essential to extend the distal segments of the ASH/ASI cilia, it is not required to build the AWB distal segments. Mutations in the *fkh-2* forkhead domain gene result in AWB-specific defects in ciliary morphology, and FKH-2 regulates kinesin-II subunit gene expression specifically in AWB. Our results suggest that cell-specific regulation of IFT contributes to the generation of ciliary diversity, and provide insights into the networks coupling the acquisition of ciliary specializations with other aspects of cell fate.

The EMBO Journal (2007) **26,** 2966–2980. doi:10.1038/sj.emboj.7601717; Published online 17 May 2007
Subject Categories: cell & tissue architecture; development
Keywords: *C. elegans*; cilia; forkhead domain; intraflagellar transport; kinesin

Introduction

Microtubule-based ciliary structures play critical roles in mediating cellular functions such as motility, sensation of environmental cues and intercellular and intracellular signal transduction in both protozoa and metazoans (Cole, 2003; Satir and Christensen, 2007; Singla and Reiter, 2006; Wang *et al*, 2006). Intraflagellar transport (IFT) motors such as kinesin and dynein build and maintain cilia by transporting ciliary axoneme precursors and membrane proteins as part of large macromolecular IFT particles (Rosenbaum and Witman, 2002; Scholey, 2003). Remarkably, the molecular motors and core components of IFT particles are highly conserved from the unicellular green alga *Chlamydomonas* to humans (Rosenbaum and Witman, 2002; Scholey, 2003). Moreover, mutations in core ciliary genes have been shown to result in a plethora of diseases such as Bardet–Biedl syndrome and polycystic kidney disease (Pazour and Rosenbaum, 2002; Eley *et al*, 2005). Thus, it is important to further characterize IFT mechanisms and to identify regulators of ciliary structure and function.

Ciliary morphologies can be highly specialized and diverse. Vertebrate sensory neurons such as olfactory neurons have eight or more elongated cilia emanating from a dendritic knob, whereas the outer segments of rod and cone photoreceptors are unique ciliary structures required for efficient phototransduction (Reese, 1965; Rohlich, 1975). Despite the critical importance of these ciliary specializations for neuron-specific sensory functions, the mechanisms required for the generation of these unique and diverse ciliary structures remain largely uncharacterized.

Caenorhabditis elegans is an excellent model system to investigate the mechanisms required for the generation of ciliary morphological diversity. In particular, 11 pairs of chemosensory neurons in the bilateral amphid organs of the head contain structurally diverse cilia. Eight of these sensory neuron types respond to aqueous attractants (Bargmann and Horvitz, 1991a, b), and contain relatively simple cilia structures consisting of one or two branches extending from the transition zone (channel cilia; Figure 1A) (Ward *et al*, 1975; Ware *et al*, 1975; Perkins *et al*, 1986). The axonemes of these cilia are comprised of a middle segment containing nine doublet peripheral microtubules and a distal segment containing nine singlet microtubules (Ward *et al*, 1975; Perkins *et al*, 1986). Three additional neuron types, AWA, AWB and AWC, respond primarily to volatile odorants (Bargmann *et al*, 1993; Troemel *et al*, 1997; Chou *et al*, 2001) and contain cilia that are morphologically unique and more elaborate (wing cilia; Figure 1A) (Ward *et al*, 1975; Ware *et al*, 1975; Perkins *et al*, 1986). The cilia of the AWA olfactory neurons are highly branched, whereas the AWB olfactory neurons contain two ciliary branches of different lengths, the distal ends of which exhibit an irregular morphology and exhibit some animal-to-animal variability (Figure 1B) (Ward *et al*, 1975; Perkins *et al*, 1986). The cilia of the AWC neurons are fan shaped and extended (Ward *et al*, 1975; Perkins *et al*, 1986). Microtubule doublets and singlets are present throughout the length of the AWC cilium and these are not organized similarly to the axoneme of the channel cilia (Evans *et al*, 2006). The ultrastructures of the AWB and AWA cilia have not been reported

*Corresponding author. Department of Biology and National Center for Behavioral Genomics, Brandeis University, 415 South Street, Waltham, MA 2454, USA. Tel.: +1 781 736 2686; Fax: +1 781 736 3107; E-mail: sengupta@brandeis.edu
[4]Present address: Department of Biology, Texas A&M University, College Station, TX, USA
[5]Present address: Department of Molecular and Cell Biology, Harvard University, Cambridge, MA 02138, USA

Received: 8 December 2006; accepted: 9 April 2007; published online: 17 May 2007

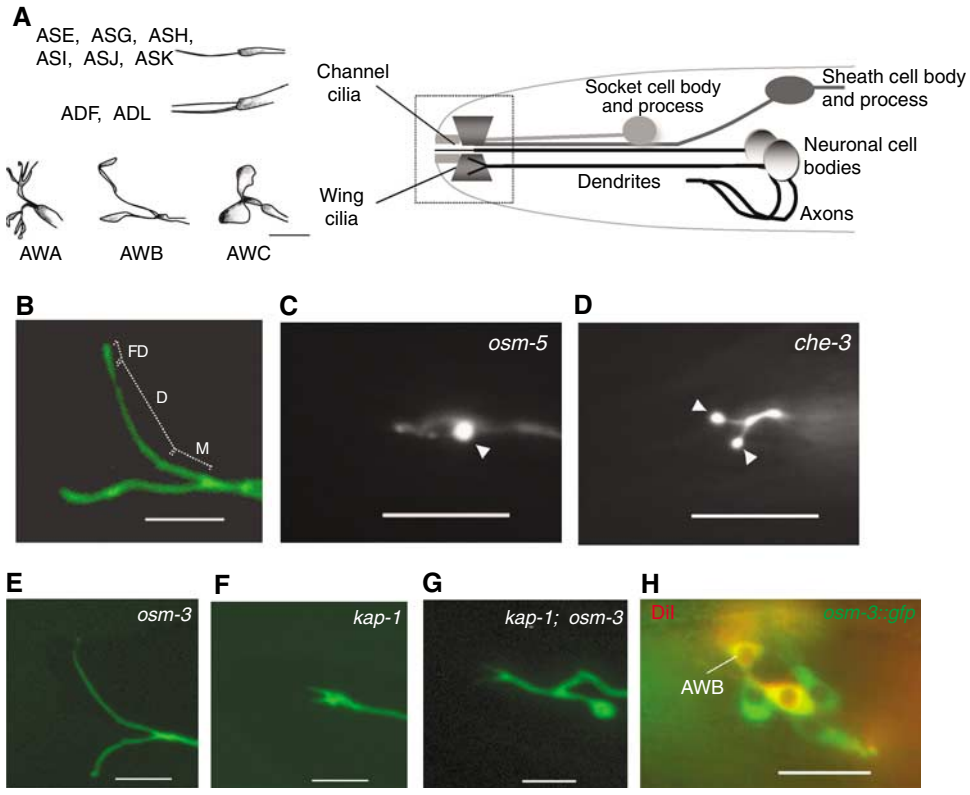

Figure 1 Effect of mutations in IFT genes and IFT motors on AWB ciliary morphology. (**A**) Diagrammatic representation of channel and wing cilia morphologies (left) and their location in the *C. elegans* head (right). (Adapted from Ward *et al*, 1975). (**B–G**) AWB cilia visualized via expression of a *str-1*p::*gfp* transgene in wild-type (panel B), *osm-5(p813)* (panel C), *che-3(e1124)* (panel D), *osm-3(p802)* (panel E), *kap-1(ok676)* (panel F) and *kap-1; osm-3* (panel G) mutant animals. Zones corresponding to ultrastructurally defined segments (Figure 2) are indicated in panel B; M, middle segment; D, distal segment; FD, far-distal segment. Arrowheads indicate accumulations at the cilia tips or base (panels C, D). Average lengths of the long and short ciliary branches were 8.0 ± 1.3 and 6.2 ± 1.3 μm (wild-type; $n = 43$), and 7.8 ± 1.3 and 6.2 ± 1.2 μm (*osm-3*; $n = 50$), respectively. (**H**) Expression of a functional *osm-3*::*gfp* fusion gene in an AWB neuron of an *osm-3* animal. AWB neurons were identified by filling with DiI. Images in panels B and E–G were acquired using a confocal microscope. Scale bars are as follows: 5 μm (panel A); 4 μm (panels B, E–G); 10 μm (panels C, D); 15 μm (panel H). Anterior is at left in all images.

in detail partly due to the complexity of their ciliary morphologies. Primary signal transduction proteins such as chemoreceptors and channels are localized to chemosensory neuron cilia (Troemel *et al*, 1995; Sengupta *et al*, 1996; Dwyer *et al*, 1998; Roayaie *et al*, 1998; Tobin *et al*, 2002), and animals with defective cilia exhibit highly compromised sensory responses (Perkins *et al*, 1986; Starich *et al*, 1995). The ability to identify and examine individual neuron types and their associated cilia provides a unique opportunity to define the developmental and cellular mechanisms required for the generation of ciliary structural diversity.

Although genetic screens have led to the identification of many molecules required for ciliary assembly in *C. elegans* (reviewed in Rosenbaum and Witman, 2002; Scholey, 2003), the mechanisms required to generate ciliary morphological diversity in *C. elegans* remain unclear. IFT has largely been visualized and quantified in all cilia simultaneously, which obscures cilia-to-cilia differences in transport mechanisms. Thus, in the channel cilia, the heterotrimeric kinesin-II and the homodimeric OSM-3 motors have been shown to act cooperatively and redundantly to elongate the doublet microtubules of the middle segments, whereas OSM-3 alone elongates the distal singlet microtubules (Snow *et al*, 2004; Ou *et al*, 2005; Pan *et al*, 2006). However, although both kinesin-II and OSM-3 are also required to build the entire AWC ciliary axoneme (Evans *et al*, 2006), no IFT was detected in the AWC neurons, and thus, it is unclear how these and other wing cilia are assembled. Little is also known about the developmental pathways that coordinate the generation of neuron-specific ciliary morphology with additional aspects of cell fate.

Here, we compare and contrast ciliary morphogenesis specifically in the AWB wing, and the ASH/ASI channel cilia. We describe the ultrastructure of the AWB cilia and show that anterograde kinesin motors function in an unexpected and cell type-specific manner to build the AWB cilia. We also identify the FKH-2 forkhead domain transcription factor as being required for the generation of AWB-specific ciliary structures and show that FKH-2 regulates expression of a kinesin-II motor subunit gene specifically in the AWB neurons. Our results provide insights into the molecules and mechanisms governing the generation of ciliary diversity and have implications on how similar specializations may be formed in other systems.

Results

Mutations in IFT particle and the dynein retrograde motor genes affect AWB and channel cilia in a similar manner

To begin to explore the roles of core ciliary genes in the formation of the AWB cilia, we first examined the AWB cilia

Table I AWB ciliary defects in core ciliary gene and *fkh-2* mutant animals

Strain	% of AWB cilia exhibiting phenotype[a]				
	Wild type	Type A[b]	Type B[c]	Shortened/absent[d]	Other
Wild type	100	0	0	0	0
osm-5(p813)	0	0	98	2	0
osm-1(p808)	0	0	88	12	0
che-11(e1810)	0	91	0	9	0
daf-10(e1387)	0	95	0	5	0
che-3(e1124)	4	96	0	0	0
xbx-1(ok279)	0	100	0	0	0
kap-1(ok676)	90	0	0	10	0
klp-11(tm324)	89	0	0	11	0
kap-1(ok676); klp-11(tm324)	88	0	0	12	0
osm-3(p802)[e]	100	0	0	0	0
kap-1(ok676); osm-3(p802)	1	0	69	30	0
fkh-2(ok683)	33	0	0	42	25[f]
fkh-2(ok683); Ex[*fkh-2 genomic*][g]	93	0	0	5	2
daf-19(m86)[h]	0	0	0	100[i]	0
daf-19(m86); fkh-2(ok683)[h]	1	0	0	88[i]	11[f]

The cilia of adult animals grown at 25°C were examined under × 400 or × 630 magnification, unless specified otherwise; $n = 30–500$ for each strain.
[a]Cilia were visualized via expression of a *str-1*p::*gfp* fusion gene, except as indicated.
[b]Type A phenotypes include shortened cilia, with accumulation at the distal tips of one or both ciliary branches, and occasionally at the base. These phenotypes are characteristic of defects in retrograde transport (Cole *et al*, 1998; Piperno *et al*, 1998).
[c]Type B phenotypes include severely shortened cilia, with accumulation at the base. These phenotypes are characteristic of defects in anterograde transport (Perkins *et al*, 1986; Cole *et al*, 1998; Haycraft *et al*, 2001).
[d]This category includes cilia, which are severely shortened or absent, with occasional ectopic projections, or cilia lacking one branch.
[e]No defects were also observed in *osm-3(hf3)* and *osm-3(mn391)* mutants.
[f]This category includes AWB neurons with prematurely terminated dendrites or neurons lacking *str-1*p::*gfp* expression.
[g]Cilia were examined via expression of *str-1*p::ODR-10::GFP in L1 larvae.
[h]The cilia of L1 larvae were examined.
[i]All ciliary structures were absent.

in animals mutant for genes previously implicated in channel cilia formation. The AWB cilia were visualized by expressing *gfp* under the AWB-specific *str-1* promoter (Troemel *et al*, 1997), which allows visualization of the soma, axonal and dendritic processes, as well as the branched AWB cilia (Figure 1B). IFT particles can be biochemically further subdivided into IFT-A and IFT-B complexes, each of which contains distinct proteins (Cole *et al*, 1998). Mutations in IFT-A complex genes result in slightly shortened channel cilia, with accumulation at the distal tips, whereas mutations in IFT-B complex genes result in severely shortened channel cilia, with accumulations at the base (Perkins *et al*, 1986; Cole *et al*, 1998). We found that mutations in the IFT-A complex gene *che-11* and *daf-10*, and the IFT-B complex genes *osm-5* and *osm-1* (Lewis and Hodgkin, 1977; Perkins *et al*, 1986; Cole *et al*, 1998; Bell *et al*, 2006), resulted in AWB cilia phenotypes similar to those of channel cilia in these mutant backgrounds (Table I; Figure 1C). In addition, mutations in the dynein retrograde motor protein gene *che-3*, and the dynein light intermediate chain gene *xbx-1*, also resulted in AWB ciliary phenotypes that resembled those exhibited by channel cilia mutants in these mutants (Albert *et al*, 1981; Schafer *et al*, 2003) (Table I; Figure 1D). Thus, the examined IFT particle component gene products and dynein appear to act via similar mechanisms in channel and AWB cilia.

Kinesin-II and OSM-3 act partly redundantly to build the AWB cilia

We next examined the roles of the anterograde heterotrimeric kinesin-II and homodimeric OSM-3 motors in the AWB cilia (Tabish *et al*, 1995; Orozco *et al*, 1999; Signor *et al*, 1999b; Snow *et al*, 2004). Consistent with previous observations, we did not observe defects in the AWB cilia in *osm-3* single mutants (Perkins *et al*, 1986) (Figure 1E; Table I). However, we observed minor defects in *kap-1* and *klp-11* kinesin-II subunit single mutants. Approximately 10% of *kap-1* or *klp-11* single mutants did not exhibit the characteristic forked structures, but instead had truncated ciliary branches, with occasional ectopic projections (Figure 1F; Table I). The phenotype was not further enhanced in *kap-1; klp-11* double mutants (Table I). AWB cilia branches were severely truncated in *kap-1; osm-3* double mutants (Figure 1G; Table I), indicating a hitherto unidentified role for OSM-3 in the assembly of these cilia. Although previous reports suggested that OSM-3 was not expressed in the AWB cilia (Tabish *et al*, 1995), we confirmed OSM-3 expression in the AWB neurons by examining expression of a functional GFP-tagged OSM-3 protein (Supplementary Table 1) driven under its own promoter (Figure 1H). These results indicate that kinesin-II and OSM-3 function partly redundantly to build the AWB ciliary axoneme.

Ultrastructure of the AWB olfactory neurons

We examined the ultrastructure of the AWB ciliary axoneme in wild-type and kinesin motor mutant backgrounds using electron microscopy. Unlike the axonemes of either the AWC or channel cilia (Perkins *et al*, 1986; Evans *et al*, 2006), the AWB axoneme in wild-type animals could be subdivided into three segments based on microtubule organization (Figure 2A). In a short middle segment (~2 μm), we noted

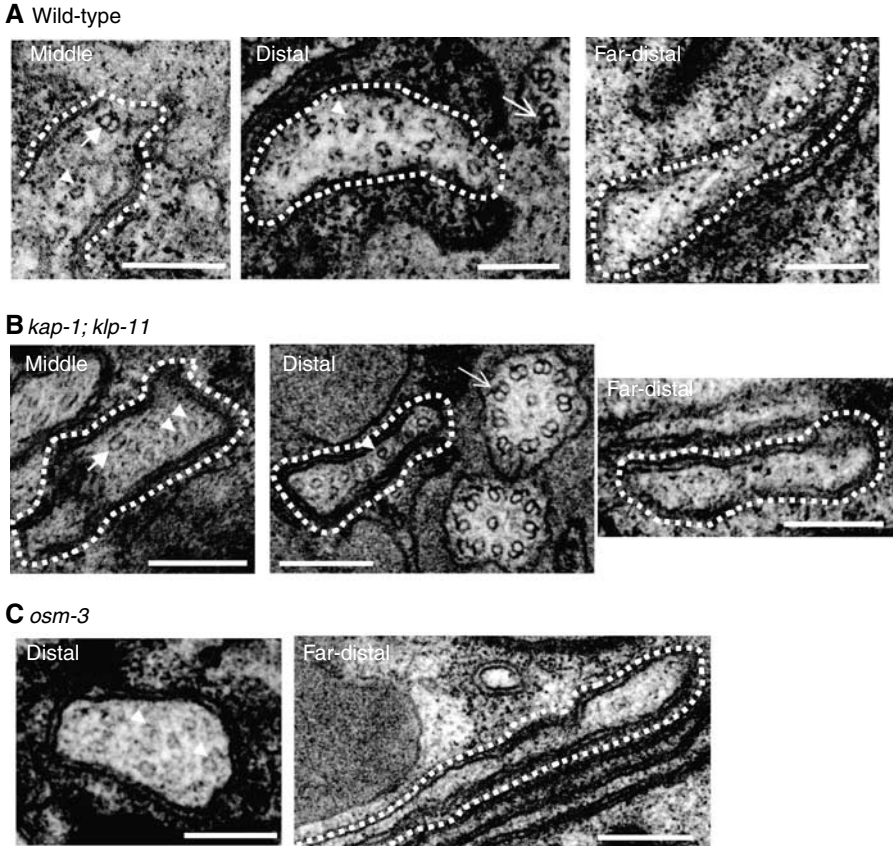

Figure 2 Ultrastructure of the AWB cilia in wild-type (**A**), *kap-1(ok676); klp-11(tm324)* (**B**) and *osm-3(p802)* (**C**) mutant animals. The cilium is outlined by a dashed line. Images were acquired at 60,000-fold magnification. Lengths of the middle, distal and far-distal segments were approximately 2, 5 and 1 μm, respectively. Arrowheads indicate singlet microtubules, closed and open arrows indicate doublet microtubules in the AWB, and channel cilia, respectively. Note the absence of an axoneme in the far-distal segment. Scale bars, 0.2 μm.

the presence of singlet microtubules and occasional doublets. In contrast to the $9+0$ arrangement of doublet microtubules in the channel cilia middle segments (Perkins *et al*, 1986), the microtubules in the AWB middle segment lacked an obvious organization. In a more elongated distal segment ($\sim$5 μm), we noted only singlet microtubules, similar to channel cilia distal segments. Finally, in the far-distal segment ($\sim$1 μm), we did not detect any microtubules, suggesting that this region, which exhibits the most animal-to-animal variability, may lack an axoneme. No gross alterations in ciliary ultrastructure were observed in either *kap-1; klp-11* double or in *osm-3* single mutant animals (Figure 2B and C). Thus, while the distal segments of channel cilia are absent in *osm-3* mutants (Perkins *et al*, 1986), formation of the distal segments of the AWB cilia does not require OSM-3.

Kinesin motors function in a cell-specific manner to build the AWB and ASH/ASI cilia

Kinesin-II and OSM-3 act together to build the middle segments of channel cilia (Snow *et al*, 2004; Ou *et al*, 2005). These motors are thought to compete with each other mechanically, resulting in an intermediate velocity of both motors in the middle segment (Snow *et al*, 2004; Pan *et al*, 2006). However, transport velocity in the distal segments is rapid due to action of the fast OSM-3 motor alone. Thus, in kinesin-II mutants, IFT velocity is accelerated in the middle segments due to the action of OSM-3, whereas in *osm-3* mutants, particles are moved at the rate of the slow kinesin-II motor movement in the middle segment (channel cilia distal segments are not formed in the absence of *osm-3*) (Snow *et al*, 2004).

To directly compare the function of kinesin motors in the channel and the AWB wing cilia, we visualized and quantified the movement of GFP-tagged KAP-1 and OSM-3 proteins specifically in the AWB and ASH/ASI neurons using the *sra-6* and *str-1* promoters (Troemel *et al*, 1995, 1997). We confirmed that both OSM-3::GFP and KAP-1::GFP fusion proteins were functional by rescuing the ciliary defects in the AWB neurons in *osm-3; kap-1* double mutants (Supplementary Table 1). In the ASH/ASI channel, as well as in the AWB wing cilia middle segments, KAP-1::GFP moved at an intermediate velocity (Figure 3A and B; Table II; Supplementary Movie S1). This velocity was reduced in *osm-3* mutants in both cilia types, albeit less markedly in the AWB middle segments (Figure 3C and D; Table II; Supplementary Movie S2), suggesting, as described previously, that kinesin-II and OSM-3 likely act together in the middle segments of both the ASH/ASI channel and AWB wing cilia.

As expected, in the ASH/ASI cilia, OSM-3::GFP moved at a slower intermediate velocity in the middle segments similar to that of KAP-1::GFP, and at a higher velocity in the distal segments (Figure 4A; Table II). Surprisingly however, OSM-3::GFP moved at a significantly higher average velocity than KAP-1::GFP in the middle segments of the AWB cilia (Figure 4B; Table II; Supplementary Movie S3),

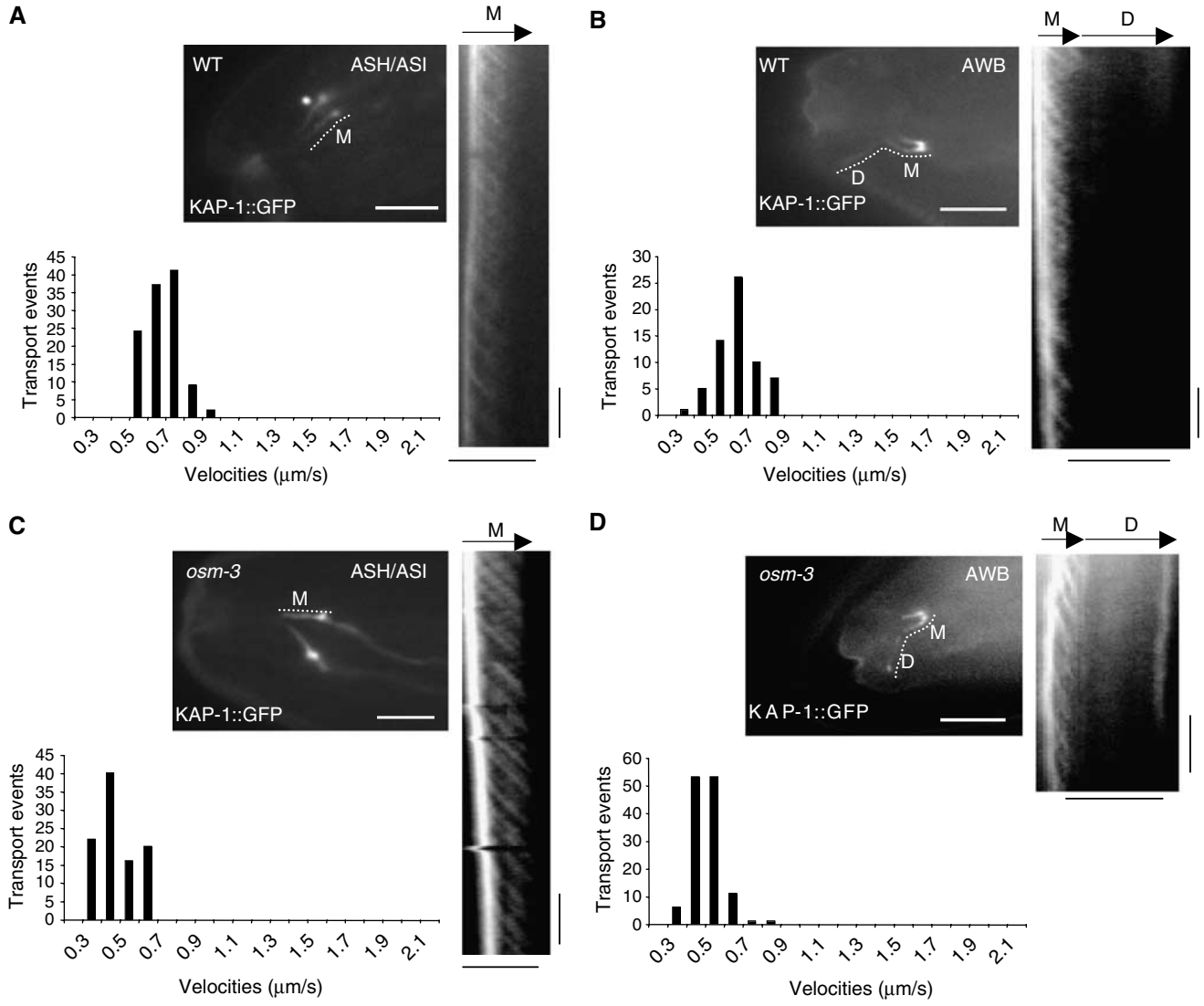

Figure 3 Movement of GFP-tagged KAP-1 in the ASH/ASI (**A, C**) and AWB (**B, D**) cilia. For each panel, still images (left) and kymographs (right) from representative movies of KAP-1::GFP transport are shown. Histograms of KAP-1::GFP velocities are shown below in each panel. For each still image, the genetic background is indicated in the top left corner, the imaged cilia in the top right corner and the fusion protein examined in the bottom left corner. Dashed lines on the still images indicate the continuous lines used to generate the kymographs. The *osm-3(p802)* allele was used. Scale bars in still images are 5 μm. Scale bars in kymographs are as follows: horizontal bar, 5 μm; vertical bar, 5 s. M, middle segment; D, distal segment. No ASH/ASI distal segments are formed in *osm-3* mutants. Statistical analyses are shown in Supplementary Tables 2 and 3.

suggesting that a subset of OSM-3::GFP molecules moves independently of kinesin-II. Consistent with this hypothesis, the velocity of OSM-3::GFP was increased by a lesser extent in kinesin-II mutants in the AWB cilia middle segments as compared with ASH/ASI cilia middle segments (Figure 4C and D; Table II; Supplementary Movie S4). Moreover, in striking contrast to the observations in ASH/ASI cilia, movement of OSM-3::GFP appeared to be largely restricted to the AWB middle segments, such that OSM-3 movement could be detected rarely in the distal segments of the AWB cilia in either wild-type or kinesin-II mutants (Figure 4B and D; Supplementary Movies S3 and S4). Taken together, these results suggest that unlike in the channel cilia, OSM-3::GFP moves partly independently of kinesin-II to build the AWB cilia middle segments, and that transport via OSM-3 may not be essential to build or maintain the AWB distal segments.

IFT mechanisms are distinct in the AWB wing and the ASH/ASI channel cilia

We next compared the movement of IFT particles in the ASH/ASI and AWB cilia by expressing the *gfp*-tagged IFT particle A and B genes *daf-10* and *osm-6* (Collet *et al*, 1998; Bell *et al*, 2006) under the *sra-6* and *str-1* promoters. We confirmed that both OSM-6::GFP and DAF-10 fusion proteins were functional by rescuing the ciliary defects in the AWB neurons in *osm-6* and *daf-10* mutants (Supplementary Table 1).

OSM-6::GFP and DAF-10::GFP moved robustly in both the middle and distal segments of the ASH/ASI channel cilia (Figure 5A; Supplementary Figure 1; Supplementary Movie S5) (Orozco *et al*, 1999; Signor *et al*, 1999a; Snow *et al*, 2004; Ou *et al*, 2005). The velocities of transport of both fusion proteins in the ASH/ASI cilia in wild-type and motor mutant backgrounds were consistent with these particles being transported by both kinesin-II and OSM-3 in the channel cilia

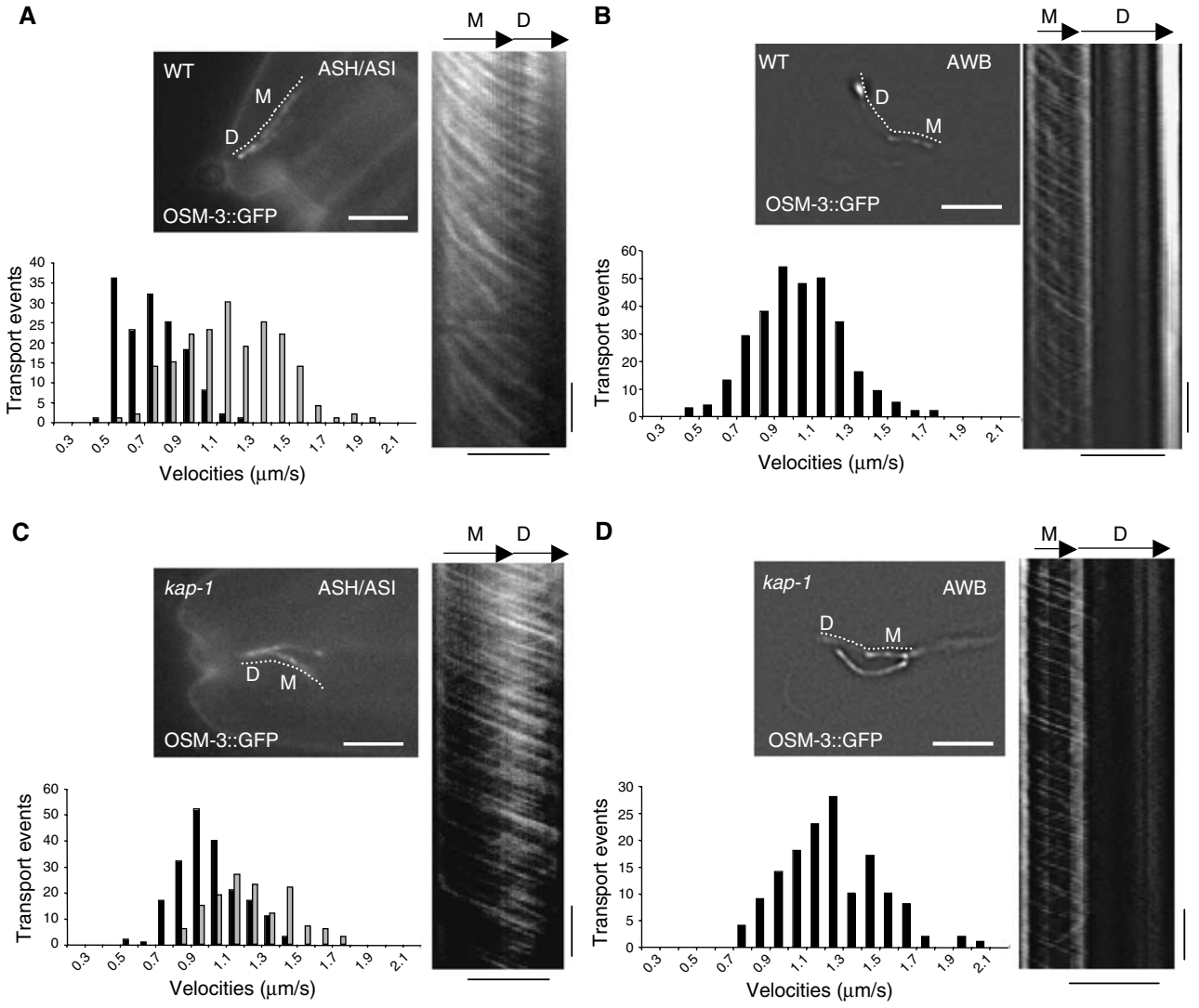

Figure 4 Movement of GFP-tagged OSM-3 in the ASH/ASI (**A, C**) and AWB (**B, D**) cilia. For each panel, still images (left) and kymographs (right) from representative movies of OSM-3::GFP transport are shown. Histograms of OSM-3::GFP velocities are shown below in each panel. Velocities in the middle (M) and distal segments (D) are indicated by black and gray bars, respectively, in each histogram. Panels are labeled as in Figure 3. The *kap-1(ok676)* allele was used. Scale bars in still images are 5 μm. Scale bars in kymographs are as follows: horizontal bar, 5 μm; vertical bar, 5 s. Statistical analyses are shown in Supplementary Tables 2 and 3.

middle segments, and by OSM-3 alone in the distal segments (Figure 5A, C and E; Table II; Supplementary Figure 1; Supplementary Movie S6).

We observed a distinct pattern of OSM-6::GFP movement in the AWB wing cilia. Although we observed robust OSM-6::GFP movement in the middle segments, we observed far fewer IFT events in the distal segments (Figure 5B; Table II; Supplementary Movie S7). DAF-10::GFP movement was also observed robustly in the middle segment but not in the distal segments (Supplementary Figure 1). Similar results were obtained with an OSM-5::GFP fusion protein, although movement of the OSM-5 fusion protein was more difficult to image due to low levels of fluorescence (Supplementary Figure 1; Table II). In the middle segments, the velocities of IFT particle fusion proteins were similar to that of kinesin-II in either wild-type or *osm-3* mutants (Table II; Figure 5B and D; Supplementary Movie S8), although we also detected a small fraction of particles moving at the higher velocity of OSM-3 alone (see histograms in Figure 5B; Supplementary Figure 1). The velocities were increased in the absence of kinesin-II (Figure 5F; Table II; Supplementary Movie S9). These results suggest that as in channel cilia middle segments, the majority of IFT particles are transported by kinesin-II and OSM-3 acting together in the AWB cilia middle segments, whereas in the absence of kinesin-II, these molecules are transported by OSM-3 alone. OSM-3 may also mediate IFT independently of kinesin-II.

Since it was surprising that few IFT events were observed in the AWB cilia distal segments, we examined this transport in more detail. Although we could image only a small number of particles due to the relative rarity of IFT events in the AWB cilia distal segments in wild-type animals, the velocity of OSM-6::GFP movement in the distal segments suggested that these particles were transported by OSM-3 (Figure 5B; Table II). Consistent with this model, we could not detect IFT events in the distal segments in *osm-3* mutants, although these segments were present (Figure 5D; Supplementary Figure 1; Supplementary Movie S8). However, in kinesin-II

Table II Anterograde velocities of IFT particles and IFT motors in ASH/ASI and AWB cilia

Fusion protein[a]	Strain background[b]	Mean velocity ($\mu m\,s^{-1} \pm$ s.d.)[c]							
		ASH/ASI				AWB			
		Middle segment	n/N[d]	Distal segment	n/N[d]	Middle segment	n/N[d]	Distal segment	n/N[d]
Motors									
KAP-1::GFP	Wild type	0.69±0.09	113/8	—[e]		0.64±0.11	63/7	—[f]	—[f]
KAP-1::GFP	*osm-3*	0.48±0.10	98/6	—[e]		0.51±0.07	125/14	—[f]	—[f]
OSM-3::GFP	Wild type	0.74±0.17	146/12	1.17±0.26	195/11	1.03±0.23	307/14	—[f]	—[f]
OSM-3::GFP	*kap-1*	1.01±0.17	196/8	1.24±0.22	140/7	1.23±0.26	146/10	—[f]	—[f]
OSM-3::GFP	*klp-11*	1.08±0.25	257/11	1.25±0.21	255/12	1.19±0.22	130/7	—[f]	—[f]
OSM-3::GFP	*fkh-2*	ND		ND		0.96±0.24	91/5	—[f]	—[f]
IFT B									
OSM-6::GFP	Wild type	0.76±0.16	253/15	1.15±0.20	286/15	0.64±0.21	274/24	0.87±0.33	50/10[g]
OSM-6::GFP	*kap-1*	1.06±0.19	291/12	1.14±0.17	235/12	1.05±0.21	135/11	1.09±0.20	135/9
OSM-6::GFP	*klp-11*	1.07±0.23	257/13	1.11±0.19	246/13	0.97±0.20	50/4	1.07±0.18	48/4
OSM-6::GFP	*osm-3*	0.48±0.11	98/5	—[e]		0.54±0.10	360/19	—[f]	—[f]
OSM-6::GFP	*fkh-2*[h]	ND		ND		0.79±0.22	61/6	0.91±0.25	69/6
OSM-5::GFP	Wild type	ND		ND		0.60±0.10	94/10	—[f]	—[f]
OSM-5::GFP	*kap-1*	ND		ND		1.08±0.32	64/7	—[f]	—[f]
IFT A									
DAF-10::GFP	Wild type	0.76±0.11	121/5	1.08±0.17	120/5	0.70±0.12	222/8	—[f]	—[f]
DAF-10::GFP	*kap-1*	ND		ND		1.20±0.28	148/11	—[f]	—[f]
DAF-10::GFP	*osm-3*	ND		—[e]		0.52±0.08	120/7	—[f]	—[f]

Movement was quantified in cilia of adult animals grown at 25°C.
ND, not done.
[a]Fusion proteins were expressed under the *sra-6* (ASH/ASI) or *str-1* (AWB) promoters.
[b]Alleles used were: *kap-1(ok676)*, *klp-11(tm324)*, *osm-3(p802)*, *fkh-2(ok683)*.
[c]Detailed statistical analyses are shown in Supplementary Tables 2 and 3.
[d]*n*, number of GFP particles; *N*, number of cilia examined.
[e]Distal segments are absent in *osm-3* mutants.
[f]Although distal segments were present, movement could not be reliably quantified, either due to complete absence or rarity of detected events.
[g]Movement of OSM-6::GFP could be quantified in the distal segments of only 10/24 examined cilia.
[h]IFT could not be visualized in severely truncated cilia in *fkh-2* animals.

mutants, we observed robust movement of OSM-6 in the AWB cilia distal segments (Table II; Figure 5F; Supplementary Movie S9). Thus, IFT does not appear to be essential to build and/or maintain the AWB distal segments in *osm-3* mutants, despite the presence of an apparently unaltered axoneme.

Mutations in the fkh-2 forkhead domain transcription factor gene affect AWB ciliary and dendritic morphology

We next sought to identify molecules that regulate AWB cilia structure. Mutations in transcription factors such as *cut* and *hamlet* have been shown to alter neuron-specific dendritic morphology in *Drosophila*, without affecting additional aspects of cell fate specification (Moore *et al*, 2002; Grueber *et al*, 2003). We reasoned that a transcription factor may act similarly in the AWB neurons to regulate the expression of genes required to generate AWB-specific ciliary morphology. The *fkh-2* forkhead domain transcription factor gene was previously shown to be broadly expressed in the embryo (Molin *et al*, 1999). However, we noted that postembryonic expression of a functional *gfp*-tagged *fkh-2* gene was restricted to the nuclei of the AWB neurons, with less consistent expression in additional chemosensory neurons (Figure 6A). *fkh-2* mutant animals were previously shown to not exhibit obvious phenotypic abnormalities, although animals doubly mutant for *fkh-2* and a second forkhead domain gene *pes-1* were embryonic lethal (Molin *et al*, 1999). Given the restricted postembryonic expression pattern of *fkh-2*, we further examined the role of *fkh-2* in the determination of AWB cell fate and function.

The *fkh-2* locus is predicted to encode two alternatively spliced transcripts (www.wormbase.org). Both transcripts are predicted to be affected in animals carrying the *ok683* deletion allele (provided by the *C. elegans* Gene Knockout Consortium) (Figure 6A), suggesting that *ok683* is a null allele. We first determined whether overall AWB cell fate specification was altered in *fkh-2* mutants by examining the expression of AWB-specific markers. *fkh-2* mutants exhibited defects in the expression of two marker::*gfp* fusion genes (Table III). These defects were markedly enhanced in animals doubly mutant for *fkh-2* and the *ceh-37 Otx* homeobox gene, which has been previously implicated in regulating AWB fate specification (Lanjuin *et al*, 2003) (Table III). Thus, FKH-2 likely acts in parallel to CEH-37 to regulate AWB cell fate.

We next determined whether mutations in FKH-2 alter AWB neuronal morphology. The dendrites of 14% of examined AWB neurons terminated prematurely in *fkh-2(ok683)* animals (Figure 6B). Dendrites terminated at different locations along the heads of animals and did not possess the characteristic ciliary structures (Figure 6B). These defects were observed as early as the three-fold embryonic stage. An additional ~40% of AWB neurons did not exhibit obvious defects in dendritic extension, but instead exhibited a range of ciliary abnormalities including shortened forks, or lack of one or both forked ciliary structures (Figure 6C; Table I). Ciliary proteins such as GFP-tagged ODR-10 and

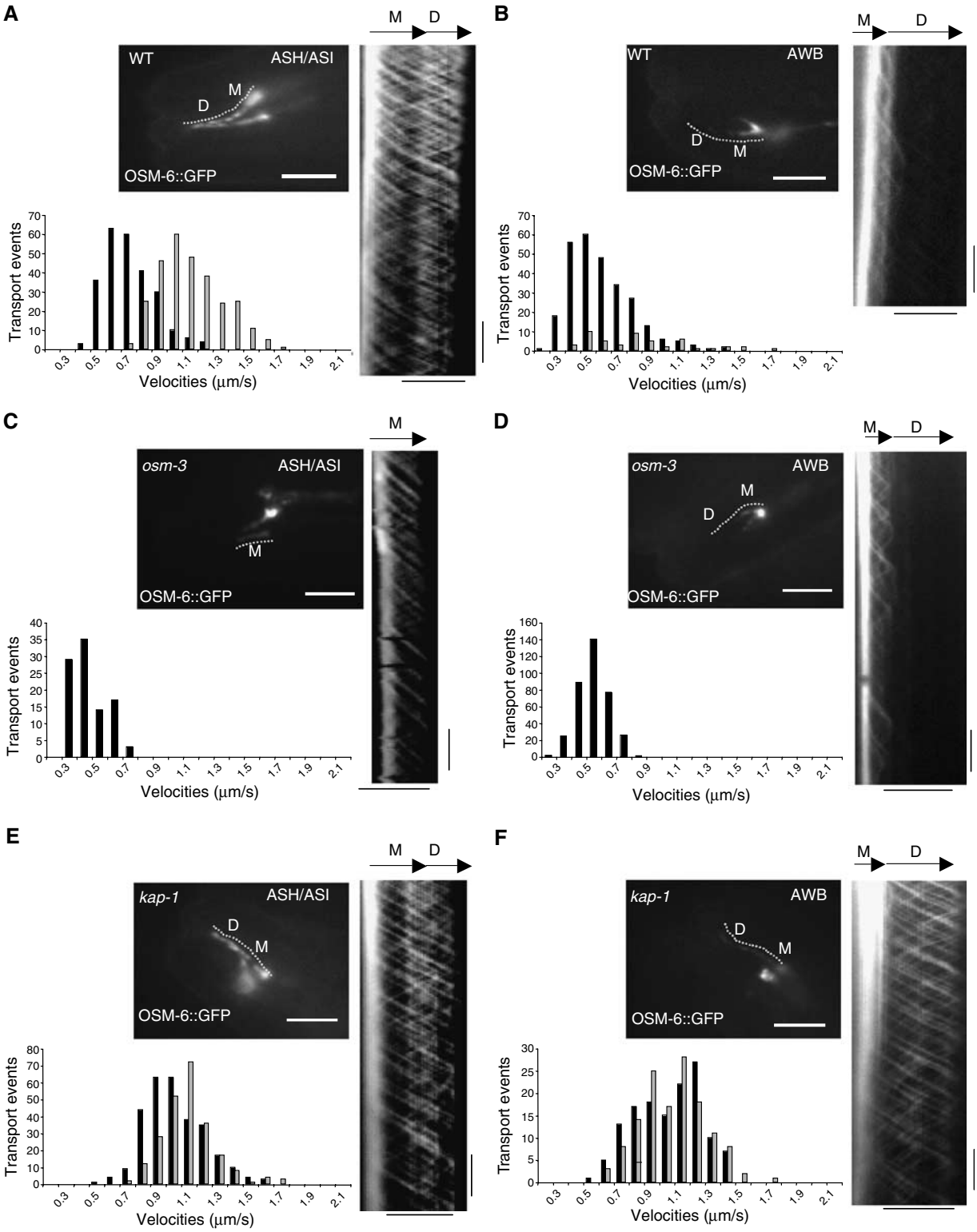

Figure 5 Movement of GFP-tagged OSM-6 in the ASH/ASI (**A, C, E**) and AWB (**B, D, F**) cilia. For each panel, still images (left) and kymographs (right) from representative movies of OSM-6::GFP transport are shown. Histograms of OSM-6::GFP velocities are shown below in each panel. Panels are labeled as in Figure 3. Velocities in the middle (M) and distal (D) segments are indicated by black and gray bars, respectively, in each histogram. Scale bars in still images are 5 μm. Scale bars in kymographs are as follows: horizontal bar, 5 μm; vertical bar, 5 s. M, middle segment; D, distal segment. No ASH/ASI distal segments are formed in *osm-3* mutants. Statistical analyses are shown in Supplementary Tables 2 and 3.

STR-1 chemoreceptors (Sengupta *et al*, 1996; Troemel *et al*, 1997) retained ciliary localization in a subset of AWB neurons exhibiting altered ciliary morphology (Figure 6D and data not shown), although no localization was observed to the ends of truncated AWB dendrites. Six pairs of amphid sensory neurons, including five channel cilia neurons and the AWB

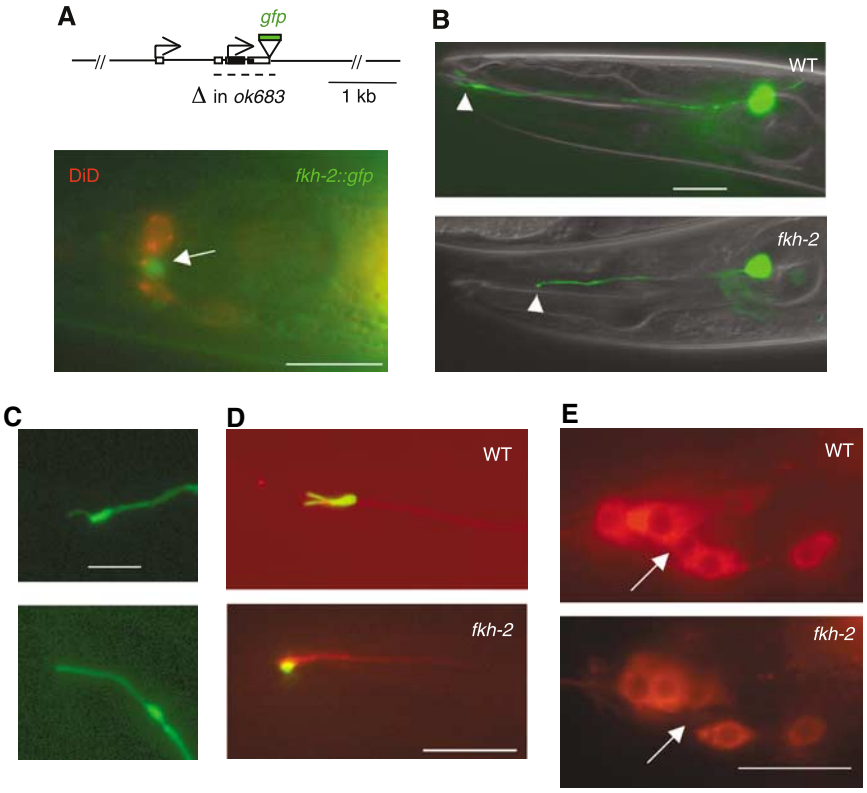

Figure 6 Mutations in *fkh-2* result in dendritic extension and ciliary defects in the AWB neurons. (**A**) A rescuing *fkh-2*::*gfp* fusion gene is expressed postembryonically in an AWB neuron (arrow) of a wild-type animal. AWB was identified by filling with the lipophilic dye DiD. The genomic organization of *fkh-2* with the location of inserted *gfp*-encoding sequences is shown at top. Arrows indicate the two predicted transcription initiation sites. Sequences encoding the forkhead domain are shaded. A dashed line indicates the extent of the *ok683* deletion. (**B**) Shown is the cell body and dendrite of an AWB neuron of a wild-type (upper panel) and *fkh-2* mutant (lower panel) adult animal expressing *str-1*p::*gfp*. Arrowheads indicate the dendrite ends. (**C**) Confocal images of AWB cilia from *fkh-2* mutant animals. Observed ciliary defects include truncated cilia (upper panel) or loss of a ciliary branch (lower panel). (**D**) Localization of a GFP-tagged ODR-10 protein to the AWB neuron cilia in wild-type (upper panel) or *fkh-2* mutants (lower panel). AWB neurons are visualized via expression of an *srd-23*p::*dsRed* fusion gene. (**E**) AWB neurons (arrow) fill with DiI in a wild-type pattern (upper panel), but fail to fill in a fraction of *fkh-2* mutants (lower panel). Scale bars are as follows: 15 μm (panels A, B, D, E); 4 μm (panel C). Anterior is at left in all images.

Table III *fkh-2* regulates AWB cell fate specification

Strain	Marker	% AWB neurons expressing
Wild type	*str-1*::*gfp*	100
fkh-2(ok683)	*str-1*::*gfp*	89
ceh-37(ok642)	*str-1*::*gfp*	45
fkh-2(ok683) ceh-37(ok642)	*str-1*::*gfp*	20
Wild type	*odr-1*::*dsRed*	100
fkh-2(ok683)	*odr-1*::*dsRed*	66[a]
ceh-37(ok642)	*odr-1*::*dsRed*	43
fkh-2(ok683) ceh-37(ok642)	*odr-1*::*dsRed*	7[a]

Expression was examined in adult animals under ×400 magnification. All marker genes were stably integrated into the genome; $n > 80$ for each.
[a]18–24% of AWC neurons exhibit dendritic extension defects in *fkh-2* mutants, such that an anteriorly directed dendrite is frequently truncated, and additionally, a posteriorly directed neurite is observed. This defect is enhanced in *fkh-2; ceh-37* double mutants in which 39% of AWC neurons exhibit dendritic extension defects.

neurons, take up lipophilic dyes such as DiI (Perkins *et al*, 1986; Herman and Hedgecock, 1990) (Figure 6E). Dye uptake is severely compromised in animals with defects in dendritic extension and ciliary morphogenesis (Perkins *et al*, 1986). Consistent with the observed dendritic and ciliary extension defects, 36% of the AWB, but not other neuron types, failed to fill with DiI in *fkh-2* mutants (Figure 6E). The dendritic and ciliary defects were rescued by a genomic fragment containing *fkh-2* coding and regulatory sequences (Table I). These results indicate that mutations in *fkh-2* regulate both AWB dendritic extension as well as AWB ciliary morphogenesis.

FKH-2 may act in the AWB neurons, or elsewhere, to regulate AWB morphology. To investigate the site of FKH-2 action, we correlated the presence or absence of *fkh-2* genomic rescuing sequences in the AWB lineage with the ability of the AWB neurons to dye-fill. The ability or failure of the AWB neurons to dye-fill correlated more highly with the presence or absence, respectively, of *fkh-2* genomic rescuing sequences in the AWB and closely related lineages than in distant lineal relatives (Sulston *et al*, 1983), suggesting that *fkh-2* acts in the AWB lineage to regulate AWB neuron morphology (see Supplementary data).

IFT is altered in the AWB cilia in fkh-2 mutants

To determine whether alterations in IFT underlie the ciliary defects observed in *fkh-2* mutants, we examined OSM-6::GFP movement in the AWB cilia of *fkh-2* mutants. Although we could not confidently image movement in severely truncated cilia, we found that in AWB cilia that could be imaged, OSM-6::GFP was transported robustly throughout the length of the cilia, whereas OSM-3::GFP movement was restricted to

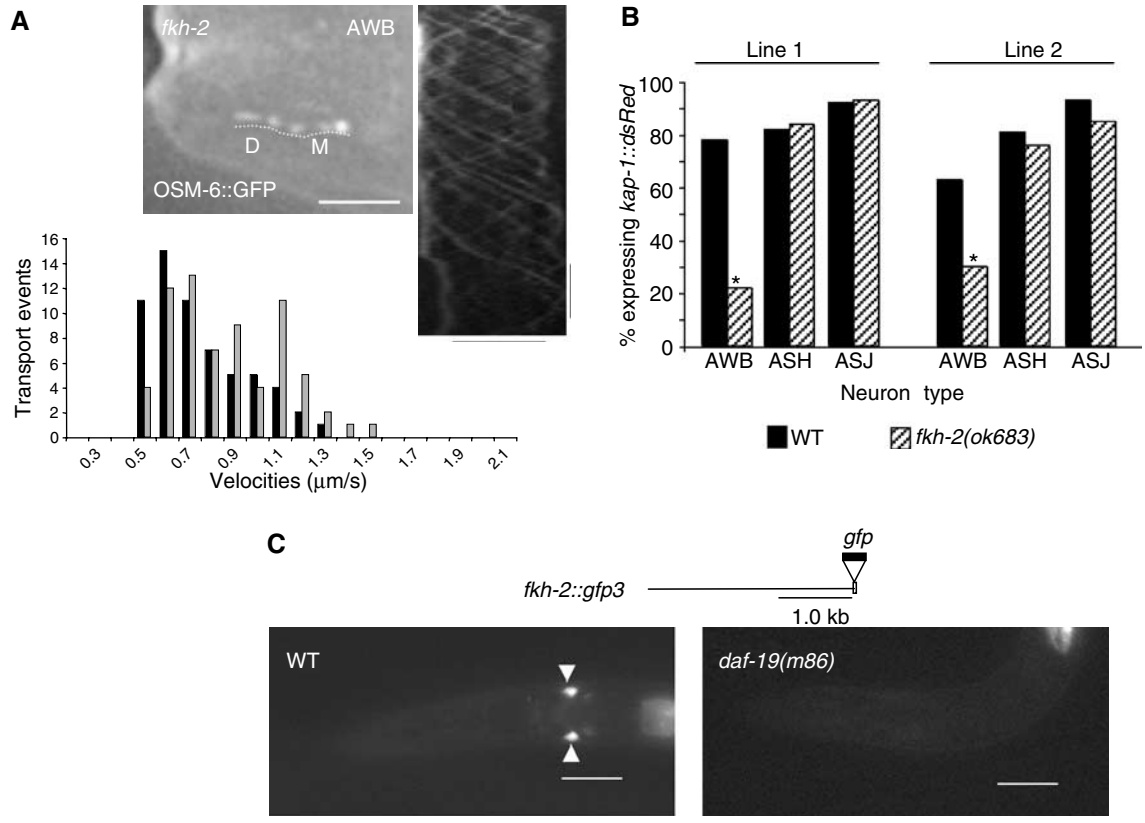

Figure 7 FKH-2 regulates *kap-1* expression in the AWB neurons. (**A**) Still image (left panel) and kymograph (right panel) from a representative movie of OSM-6::GFP in an AWB cilia of a *fkh-2(ok683)* animal. Histograms of OSM-6::GFP velocities are shown below. Dashed lines on the still images indicate the continuous lines used to generate the kymographs. Velocities in the middle (M) and distal (D) segments are indicated in black and gray bars, respectively. Scale bar in the still image is 5 μm. Scale bars in kymographs are as follows: horizontal bar, 5 μm; vertical bar, 5 s. (**B**) Shown are the percentages of the indicated chemosensory neuron types expressing *kap-1*p::*dsRed* in wild-type or *fkh-2(ok683)* animals. Numbers shown are from two independent transgenic lines expressing *kap-1*p::*dsRed* from extrachromosomal arrays. Asterisk indicates values that are different from WT at $P<0.001$ using a chi-square test. (**C**) A *fkh-2*::*gfp (IeIs916)* fusion construct is expressed in the AWB (arrowheads) and additional neurons in wild-type animals (left panel) but not in *daf-19(m86)* mutants (right panel). A total of 100% of *daf-19* mutants failed to express *fkh-2*::*gfp* ($n=119$) compared with 0% of wild-type animals ($n=31$) in the L1 developmental stage. Scale bars, 15 μm. Anterior is to the left in both images.

the AWB middle segments, similar to our observations in *kap-1* mutants (Figure 7A; Table II; Supplementary Movie S10). This result suggests that FKH-2 may act in part by altering *kap-1* gene expression. However, the velocity of OSM-6::GFP movement in the AWB middle segments in *fkh-2* mutants was significantly different from that in *kap-1* mutant animals (Table II), suggesting that *kap-1* expression may not be fully lost in *fkh-2* mutants.

To test this hypothesis, we examined the expression of *kap-1*p::*dsRed* in *fkh-2(ok683)* mutants. We found that *kap-1* expression was significantly downregulated but not abolished in the AWB neurons of *fkh-2* mutants relative to wild-type animals (Figure 7B). Expression in two additional neuron types (ASH and ASJ) was unaltered. We next correlated downregulation of *kap-1* expression with defects in ciliary and dendritic structures. A total of 87% of animals exhibiting dendritic and/or ciliary defects also exhibited loss of *kap-1*p::*dsRed* expression in the AWB neurons ($n=126$). However, we also observed wild-type morphology in AWB neurons lacking *kap-1* expression. *fkh-2; kap-1* double mutants exhibited cilia and dendrite defects similar to those of *fkh-2* mutants alone (data not shown). Taken together with the observation that *kap-1* mutants exhibit weaker AWB morphological defects than *fkh-2* mutants, these results suggest that *kap-1* represents one of a larger set of FKH-2 target genes that regulate AWB dendritic and ciliary morphology.

The RFX transcription factor DAF-19 regulates fkh-2 expression postembryonically in the AWB neurons

The RFX transcription factor DAF-19 has been shown to regulate ciliogenesis such that all ciliated neurons lack cilia in *daf-19* mutants (Perkins *et al*, 1986; Swoboda *et al*, 2000). We examined the regulatory relationship, if any, between DAF-19 and FKH-2. We observed a dramatic downregulation of postembryonic *fkh-2* expression in *daf-19* mutants (Figure 7C), although embryonic expression appeared grossly unaltered. DAF-19 regulates the transcription of target genes via binding a conserved X box sequence (Swoboda *et al*, 2000). We identified a low-probability X box element in the promoter of *fkh-2*, which is also conserved in the *fkh-2* ortholog in the related nematode *Caenorhabditis briggsae*. However, mutating this sequence did not abolish *fkh-2* expression (data not shown), suggesting that DAF-19 binds alternate sites or acts via intermediate molecules to regulate *fkh-2* expression. The AWB cilia of *daf-19; fkh-2* mutant animals exhibited defects similar to those of *daf-19* mutants alone (Table I). However, unlike *fkh-2* mutants, we did not

observe defects in AWB dendritic extension in *daf-19* mutants, and *daf-19; fkh-2* double mutants had dendritic defects similar to *fkh-2* mutants (Table I). These results suggest that DAF-19-mediated regulation of FKH-2 expression plays a role in AWB ciliogenesis, but that DAF-19-independent expression of FKH-2 may regulate AWB dendritic morphology.

Discussion

Deployment of IFT mechanisms in a cell-specific manner may generate ciliary structural diversity

Direct visualization of IFT and motor movement in cilia *in vivo* has allowed the identification and description of the dynamics of cilia formation and maintenance (Rosenbaum and Witman, 2002; Scholey, 2003). However, in *C. elegans*, IFT has previously been examined in multiple cilia at once (Orozco *et al*, 1999), precluding the identification of cell-to-cell differences in IFT mechanisms. Here, we examine and quantify IFT specifically in two cilia types, by driving expression of motor and IFT particle genes specifically in the ASH/ASI channel, and in the AWB wing cilia using cell-specific promoters. This approach has allowed us, for the first time, to compare and contrast IFT mechanisms in cilia of two different morphologies, and to uncover cell-specific mechanisms that may contribute to the generation of ciliary morphological diversity.

The ultrastructures of the channel cilia and the AWB wing cilia are grossly similar in that the middle segments contain doublet microtubules and the distal segments contain singlets (Perkins *et al*, 1986; this work). However, there are also differences in the axoneme structures of these cilia. Unlike in the channel cilia, the middle segment of the AWB cilium is relatively short and contains rare doublets as well as singlet microtubules that are not organized in the typical cylindrical structure. In addition, distal segments of the AWB cilium are elongated as compared with the distal segments of the channel cilia. Finally, the far-distal region of the AWB cilium appears to lack a central axoneme, raising the possibility that this structure is simply a membraneous extension. The AWC ciliary axoneme was previously shown to contain both doublet and singlet microtubules throughout the length of the cilium (Evans *et al*, 2006). Thus, differences in axoneme structure underlie the observed morphological diversity in *C. elegans* sensory neuron cilia.

Modulation of IFT and motor protein function in a cell-specific manner likely contributes to the differences in axoneme structure, and hence, morphological diversity. Previous studies have suggested that the conserved heterotrimeric kinesin-II is the core ciliary anterograde motor, whereas the homodimeric OSM-3 kinesin acts as an 'accessory' motor that can act with or substitute for kinesin-2, and also elongates distal segments containing singlet microtubules (Snow *et al*, 2004; Evans *et al*, 2006). However, OSM-3 appears to be deployed in a distinct manner in the AWB cilia. Although a subset of OSM-3 molecules acts with kinesin-II in the AWB cilia middle segments to mediate IFT, unlike in the channel cilia, OSM-3 also appears to act in a kinesin-II-independent manner. Components of both IFT particle A and B complexes appear to be transported largely by kinesin-II/OSM-3 acting together, although a small subset may be transported by OSM-3 alone (Figure 8A). OSM-3 may

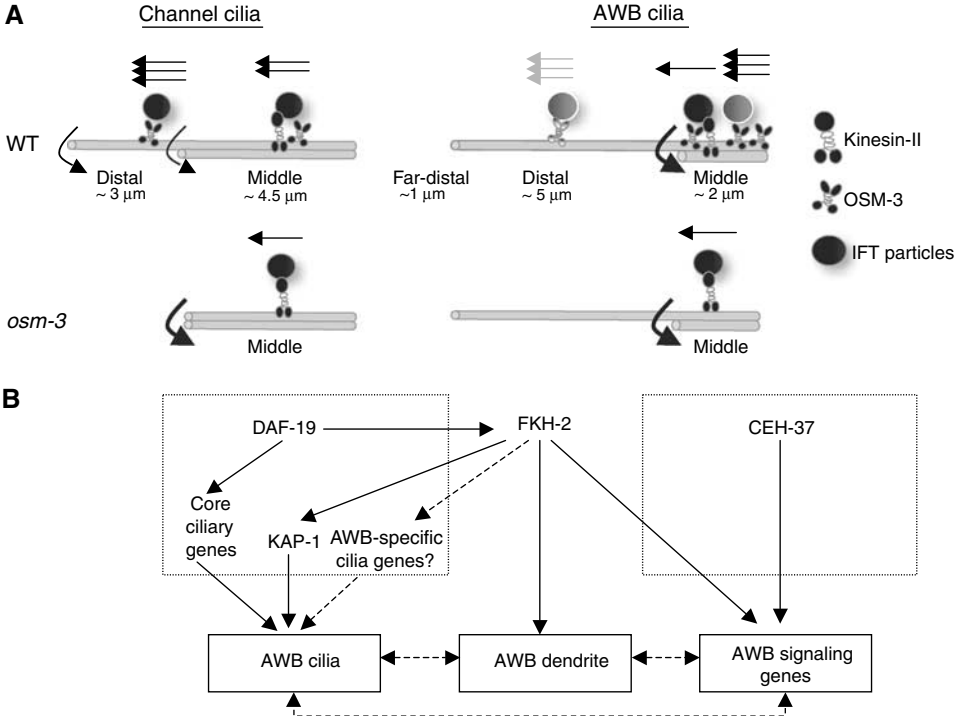

Figure 8 Cell-specific modulation of IFT may generate ciliary diversity. (**A**) Models comparing IFT in the channel and AWB cilia. Number of arrows are directly proportional to measured velocity. Note that distal segments are absent in channel but not in AWB cilia in *osm-3* mutants. In the AWB middle segments, OSM-3 is proposed to function partly independently of kinesin-II. We detected IFT events and motor movement in the AWB distal segments rarely in wild-type or *osm-3* mutant cilia, suggesting that the majority of motor proteins and IFT particles may undergo turnaround (represented by a curved arrow) at the middle/distal segment border in AWB cilia. See text for additional details. (**B**) Model of FKH-2 function in fate specification of the AWB neurons. FKH-2 may link a ciliogenic module (left box) with an AWB-specific developmental module (right box) to generate AWB-specific morphology and AWB fate. Dashed lines indicate postulated regulatory relationships.

also transport a partly distinct set of cargo proteins in the AWB cilia. The mammalian homolog of OSM-3 is required for ciliary targeting of olfactory cyclic nucleotide-gated channel subunits in mammalian cells (Jenkins *et al*, 2006), suggesting that OSM-3 may be responsible for ciliary targeting of cell-specific proteins. We note that OSM-3 cannot fully substitute for loss of kinesin-II function, such that a small fraction of *kap-1/klp-11* mutants continue to exhibit severely truncated AWB cilia. This observation further supports the hypothesis that OSM-3 acts as an accessory motor.

A particularly striking difference in the deployment of OSM-3 in the AWB and channel cilia is the requirement of this motor in forming the distal ciliary segments. Although both the channel cilia and AWB cilia distal segments contain singlet microtubules, OSM-3 is required to form these segments in the channel but not in the AWB cilia. Thus, in *osm-3* mutants, the distal segments of the channel cilia are absent (Perkins *et al*, 1986), whereas the distal segments of the AWB cilia are unaffected. Moreover, unlike in the channel cilia, we did not detect robust movement of either OSM-3 or IFT particle proteins in the AWB cilia distal segments. This observation further corroborates the hypothesis that OSM-3 may not be essential to form the AWB ciliary distal segments.

We envision several mutually non-exclusive possibilities to account for our observations. The majority of motor molecules and IFT particles may undergo turnaround at the border between the middle and distal segments in the AWB cilia and are transported retrogradely to the ciliary base (Figure 8A), much like the case at the flagellar tip in *Chlamydomonas* (Sloboda, 2005; Pedersen *et al*, 2006). This would result in a decrease in the number of IFT particles and OSM-3 motors in the distal segments. The IFT particle composition and cargoes may also undergo drastic alterations at the middle/distal segment border, such that the IFT components OSM-5, OSM-6 and DAF-10 are largely excluded from the distal segments. It is also possible that the AWB distal segments are elongated in an IFT-independent manner, or that IFT is required transiently early in ciliary assembly to generate the distal segments, but is not essential at other stages to maintain ciliary structure.

A puzzling observation was the robust transport of OSM-6::GFP in AWB cilia distal segments in kinesin-II mutants, in the absence of corresponding robust movement of the OSM-3 motor in this region. The IFT protein particle composition may be altered in kinesin-II mutants, such that more IFT particle proteins are transported per OSM-3 motor molecule in the distal segments, allowing us to visualize robust movement. It is also possible that this altered pattern may reflect the use of an alternate motor protein in the distal segments in a kinesin-II mutant background. Proteins regulating kinesin motor functions have been identified in *C. elegans* (Blacque *et al*, 2004; Ou *et al*, 2005). Cell-specific regulation of motor protein function is likely to underlie these cell-specific differences in kinesin-II and OSM-3 function, and hence, ciliary structures.

The FKH-2 transcription factor couples AWB cell fate specification with the acquisition of cell-specific ciliary morphology

Our results suggest that the core ciliogenic program is likely to be modulated in a cell-specific manner, so as to promote the generation of unique ciliary structures. In the AWB neurons, we have identified the FKH-2 forkhead domain transcription factor as being an important link between the developmental programs that specify cell fate with the ciliogenic program that is common to all ciliated neurons (Figure 8B). FKH-2 acts synergistically with the OTX homeodomain protein CEH-37 (Lanjuin *et al*, 2003) to specify AWB cell fate, but in addition, regulates the expression of broadly expressed ciliary genes such as *kap-1* in an AWB-specific manner. It is unlikely that *kap-1* is the sole target of FKH-2 in the regulation of ciliogenesis in AWB, since downregulation of *kap-1* expression is not sufficient to account for all *fkh-2* ciliary phenotypes. We propose that FKH-2 regulates additional genes in an AWB-specific manner, a subset of which modulates IFT mechanisms. *fkh-2* expression, is in turn regulated by the DAF-19 RFX transcription factor (Figure 8B). A similar developmental network has been described for the male-specific HOB neurons in *C. elegans*, where an as yet unidentified factor has been proposed to couple the DAF-19-regulated ciliogenic program, with other aspects of HOB cell fate regulated by the transcription factors EGL-44 and EGL-46 (Yu *et al*, 2003). It is interesting to note that although *fkh-2* mutants also exhibit AWB dendritic morphological abnormalities, the functions of FKH-2 in regulating dendritic structure are independent of DAF-19. Thus, FKH-2 acts in both DAF-19-dependent and independent pathways to regulate AWB morphology.

In mice, the forkhead domain transcription factor HFH-4/FOXJ1 has been implicated in the generation of a subclass of motile cilia. *hfh-4* is expressed in epithelial cells in the embryonic node, which contain motile monocilia required for the generation of left–right asymmetry (Nonaka *et al*, 1998; Marszalek *et al*, 1999; Takeda *et al*, 1999), and also in ciliated epithelial cells in the airway and other tissues during ciliogenesis (Hackett *et al*, 1995; Lim *et al*, 1997; Blatt *et al*, 1999; Tichelaar *et al*, 1999). *hfh-4*-null mice lack motile airway cilia due to defective migration or anchoring of the basal bodies, and exhibit left–right asymmetry defects due to dysfunction of node cilia, perhaps in part via regulation of dynein (Chen *et al*, 1998; Brody *et al*, 2000; Gomperts *et al*, 2004). Thus, similar to FKH-2, HFH-4 also regulates the generation and function of specific ciliary structures. It remains to be determined whether other forkhead domain proteins play roles in similar aspects of cell-specific ciliogenesis.

Diversity of ciliary structure ensures maximal optimization of cell functions. The precise topographic arrangement and compartmentalization of cell-specific sensory receptors and signaling molecules in the cilia are essential for accurate and sensitive detection and signal transduction of external cues (Young and Droz, 1968; Kulaga *et al*, 2004; Nishimura *et al*, 2004; Corbit *et al*, 2005; Haycraft *et al*, 2005; Peden and Barr, 2005; Qin *et al*, 2005; Flannery *et al*, 2006; Wang *et al*, 2006). Results described here provide insights into the mechanisms by which the appropriate ciliary specializations may be generated via cell-specific modulation of core ciliary proteins, and describe how the acquisition of ciliary structures may be coupled with additional aspects of cell fate specification.

Materials and methods

Nematode strains

Strains were obtained from the *Caenorhabditis* Genetics Center or the National Bioresource Project (Japan). *fkh-2(ok683)* was

outcrossed eight times before analysis and the extent of the deletion was verified by amplification. Stably integrated strains used in this work were: *kyIs104* (*str-1*p::*gfp*) (Troemel *et al*, 1997), *kyIs156* (*str-1*p::*odr-10cDNA*::*gfp*), *oyIs44* (*odr-1*p::*dsRed*) (Lanjuin *et al*, 2003) and *IeIs916* (*fkh-2*::*gfp*) (Molin *et al*, 2000; gift from I Hope). Double mutants were constructed using standard methods and the presence of individual mutations was verified by complementation and/or amplification, and sequencing of genomic sequences.

Microscopy

Images were acquired on a Zeiss Axioplan microscope using a $\times 40$ (1.30 NA) or $\times 63$ (1.25 NA) objective at room temperature and a CCD camera (Hamamatsu), and analyzed using Openlab 4.0 software (Improvision). Confocal images were acquired using a $\times 100$ (1.4 NA) objective on a Leica spectral confocal microscope, and analyzed using Leica imaging software.

For quantification of IFT particle and motor movement, transgenic animals were anesthetized with 10 mM levamisole and mounted on agarose pads before imaging. Movies were obtained with a Nikon Eclipse TE2000 microscope equipped with a $\times 100$ (1.4 NA) objective and a forced air-cooled Photometrics Cascade 512B with a CCD87 CCD. All images for IFT particle and motor movement were collected at 200 ms frame^{-1} at room temperature. Kymographs and movies were generated using the Metamorph software package (Molecular Devices). Stacks of images for movies of movement in the AWB cilia shown in Figure 4 were further processed by unsharp masking, low-pass filtering and edge detecting, and presented after autoscaling using Metamorph software.

Molecular biology and generation of transgenic strains

str-1 or *sra-6* promoter driven *gfp*-tagged *osm-6, osm-5, daf-10, osm-3 (M02B7.3b), kap-1* and *fkh-2* cDNA constructs were generated by fusing ~3 kb of *str-1* or *sra-6* upstream promoter sequences with the respective *gfp*-tagged cDNAs in a modified *C. elegans* expression vector. The *srd-23*p::*dsRed* plasmid was generated by fusing ~3 kb of *srd-23* upstream promoter sequences to *dsRed* and *gfp*-tagged *fkh-2-gfp* constructs were generated by cloning *fkh-2* promoter, coding and 3′-UTR genomic sequences into *C. elegans gfp* expression vectors. *kap-1*p::*dsRed* was generated by PCR fusion (Hobert, 2002) of *dsRed* coding sequences with ~212 bp of *kap-1* upstream sequences. A functional *gfp*-tagged *osm-3* gene was generated by fusing *gfp* sequences in frame to *osm-3* genomic sequences including 1.9 kb upstream promoter sequences (Hobert, 2002). Plasmid constructs were verified by sequencing. *C. elegans* expression vectors were gifts from A Fire and were modified by M Colosimo. Transgenic strains were generated using *unc-122*::*dsRed* as the co-injection marker.

Statistical analyses

Statistical analyses of IFT particle and motor protein velocities were performed using one-way ANOVA and Scheffe's *post hoc* multiple comparison tests between all possible pairs in each data set using the SPSS 14 statistical analyses package.

Electron microscopy

Adult hermaphrodites were fixed in 3% gluteraldehyde on ice for 2 h, followed by a post fix in 1% OsO_4 for 1 h at room temperature. Animals were then processed for electron microscopy as previously described (Bargmann *et al*, 1993). Sections measuring 50 nm were serially collected from the tip of the nose.

Supplementary data

Supplementary data are available at *The EMBO Journal* Online (http://www.embojournal.org).

Acknowledgements

We are indebted to Joel Rosenbaum for his insights and enthusiasm, and for hosting SM in his laboratory. We are grateful to Ian Hope for directing our attention to the *fkh-2* expression pattern, Mayumi Shibuya and Caron Gauthier for technical assistance, David Hall and Cori Bargmann for interpretation of micrographs, Don Katz for help with statistics, Guangshuo Ou, Jonathan Scholey and the Sengupta laboratory for discussions, and Joel Rosenbaum and Paul Garrity for comments on the manuscript. We thank the *Caenorhabditis* Genetics Center, *C. elegans* Knockout Consortium and Shohei Mitani at the National Bioresource Project (Japan) for strains. This work was supported by the NIH (GM56223 – PS; S10RR16708 and P30NS45713) and the Klingenstein Fund for Neuroscience (SS).

References

Albert PS, Brown SJ, Riddle DL (1981) Sensory control of dauer larva formation in *Caenorhabditis elegans*. *J Comp Neurol* **198:** 435–451

Bargmann CI, Hartwieg E, Horvitz HR (1993) Odorant-selective genes and neurons mediate olfaction in *C. elegans*. *Cell* **74:** 515–527

Bargmann CI, Horvitz HR (1991a) Chemosensory neurons with overlapping functions direct chemotaxis to multiple chemicals in *C. elegans*. *Neuron* **7:** 729–742

Bargmann CI, Horvitz HR (1991b) Control of larval development by chemosensory neurons in *Caenorhabditis elegans*. *Science* **251:** 1243–1246

Bell LR, Stone S, Yochem J, Shaw JE, Herman RK (2006) The molecular identities of the *Caenorhabditis elegans* intraflagellar transport genes *dyf-6, daf-10* and o*sm-1*. *Genetics* **173:** 1275–1286

Blacque OE, Reardon MJ, Li C, McCarthy J, Mahjoub MR, Ansley SJ, Badano JL, Mah AK, Beales PL, Davidson WS, Johnsen RC, Audeh M, Plasterk RH, Baillie DL, Katsanis N, Quarmby LM, Wicks SR, Leroux MR (2004) Loss of *C. elegans* BBS-7 and BBS-8 protein function results in cilia defects and compromised intraflagellar transport. *Genes Dev* **18:** 1630–1642

Blatt EN, Yan XH, Wuerffel MK, Hamilos DL, Brody SL (1999) Forkhead transcription factor HFH-4 expression is temporally related to ciliogenesis. *Am J Respir Cell Mol Biol* **21:** 168–176

Brody SL, Yan XH, Wuerffel MK, Song SK, Shapiro SD (2000) Ciliogenesis and left–right axis defects in forkhead factor HFH-4-null mice. *Am J Respir Cell Mol Biol* **23:** 45–51

Chen J, Knowles HJ, Hebert JL, Hackett BP (1998) Mutation of the mouse hepatocyte nuclear factor/forkhead homologue 4 gene results in an absence of cilia and random left–right asymmetry. *J Clin Invest* **102:** 1077–1082

Chou JH, Bargmann CI, Sengupta P (2001) The *Caenorhabditis elegans odr-2* gene encodes a novel Ly-6-related protein required for olfaction. *Genetics* **157:** 211–224

Cole DG (2003) The intraflagellar transport machinery of *Chlamydomonas reinhardtii*. *Traffic* **4:** 435–442

Cole DG, Diener DR, Himelblau AL, Beech PL, Fuster JC, Rosenbaum JL (1998) *Chlamydomonas* kinesin-II-dependent intraflagellar transport (IFT): IFT particles contain proteins required for ciliary assembly in *Caenorhabditis elegans* sensory neurons. *J Cell Biol* **141:** 993–1008

Collet J, Spike CA, Lundquist EA, Shaw JE, Herman RK (1998) Analysis of *osm-6*, a gene that affects sensory cilium structure and sensory neuron function in *Caenorhabditis elegans*. *Genetics* **148:** 187–200

Corbit KC, Aanstad P, Singla V, Norman AR, Stainier DY, Reiter JF (2005) Vertebrate smoothened functions at the primary cilium. *Nature* **437:** 1018–1021

Dwyer ND, Troemel ER, Sengupta P, Bargmann CI (1998) Odorant receptor localization to olfactory cilia is mediated by ODR-4, a novel membrane-associated protein. *Cell* **93:** 455–466

Eley L, Yates LM, Goodship JA (2005) Cilia and disease. *Curr Opin Genet Dev* **15:** 308–314

Evans JE, Snow JJ, Gunnarson AL, Ou G, Stahlberg H, McDonald KL, Scholey JM (2006) Functional modulation of IFT kinesins extends the sensory repertoire of ciliated neurons in *Caenorhabditis elegans*. *J Cell Biol* **172:** 663–669

Flannery RJ, French DA, Kleene SJ (2006) Clustering of cyclic-nucleotide-gated channels in olfactory cilia. *Biophys J* **91:** 179–188

Gomperts BN, Gong-Cooper X, Hackett BP (2004) Foxj1 regulates basal body anchoring to the cytoskeleton of ciliated pulmonary epithelial cells. *J Cell Sci* **117:** 1329–1337

Grueber WB, Jan LY, Jan YN (2003) Different levels of the homeodomain protein cut regulate distinct dendrite branching patterns of *Drosophila* multidendritic neurons. *Cell* **112:** 805–818

Hackett BP, Brody SL, Liang M, Zeitz ID, Bruns LA, Gitlin JD (1995) Primary structure of hepatocyte nuclear factor/forkhead homologue 4 and characterization of gene expression in the developing respiratory and reproductive epithelium. *Proc Natl Acad Sci USA* **92:** 4249–4253

Haycraft CJ, Banizs B, Aydin-Son Y, Zhang Q, Michaud EJ, Yoder BK (2005) Gli2 and Gli3 localize to cilia and require the intraflagellar transport protein polaris for processing and function. *PLoS Genet* **1:** e53

Haycraft CJ, Swoboda P, Taulman PD, Thomas JH, Yoder BK (2001) The *C. elegans* homolog of the murine cystic kidney disease gene Tg737 functions in a ciliogenic pathway and is disrupted in *osm-5* mutant worms. *Development* **128:** 1493–1505

Herman RK, Hedgecock EM (1990) Limitation of the size of the vulval primordium of *Caenorhabditis elegans* by *lin-15* expression in surrounding hypodermis. *Nature* **348:** 169–171

Hobert O (2002) PCR fusion-based approach to create reporter gene constructs for expression analysis in transgenic *C. elegans*. *Biotechniques* **32:** 728–730

Jenkins PM, Hurd TW, Zhang L, McEwen DP, Brown RL, Margolis B, Verhey KJ, Martens JR (2006) Ciliary targeting of olfactory CNG channels requires the CNGB1b subunit and the kinesin-2 motor protein, KIF17. *Curr Biol* **16:** 1211–1216

Kulaga HM, Leitch CC, Eichers ER, Badano JL, Lesemann A, Hoskins BE, Lupski JR, Beales PL, Reed RR, Katsanis N (2004) Loss of BBS proteins causes anosmia in humans and defects in olfactory cilia structure and function in the mouse. *Nat Genet* **36:** 994–998

Lanjuin A, VanHoven MK, Bargmann CI, Thompson JK, Sengupta P (2003) *Otx/otd* homeobox genes specify distinct sensory neuron identities in *C. elegans*. *Dev Cell* **5:** 621–633

Lewis JA, Hodgkin JA (1977) Specific neuroanatomical changes in chemosensory mutants of the nematode *Caenorhabditis elegans*. *J Comp Neurol* **172:** 489–510

Lim L, Zhou H, Costa RH (1997) The winged helix transcription factor HFH-4 is expressed during choroid plexus epithelial development in the mouse embryo. *Proc Natl Acad Sci USA* **94:** 3094–3099

Marszalek JR, Ruiz-Lozano P, Roberts E, Chien KR, Goldstein LS (1999) Situs inversus and embryonic ciliary morphogenesis defects in mouse mutants lacking the KIF3A subunit of kinesin-II. *Proc Natl Acad Sci USA* **96:** 5043–5048

Molin L, Mounsey A, Aslam S, Bauer P, Young J, James M, Sharma-Oates A, Hope IA (2000) Evolutionary conservation of redundancy between a diverged pair of forkhead transcription factor homologues. *Development* **127:** 4825–4835

Molin L, Schnabel H, Kaletta T, Feichtinger R, Hope IA, Schnabel R (1999) Complexity of developmental control: analysis of embryonic cell lineage specification in *Caenorhabditis elegans* using *pes-1* as an early marker. *Genetics* **151:** 131–141

Moore AW, Jan LY, Jan YN (2002) hamlet, a binary genetic switch between single—and multiple—dendrite neuron morphology. *Science* **297:** 1355–1358

Nishimura DY, Fath M, Mullins RF, Searby C, Andrews M, Davis R, Andorf JL, Mykytyn K, Swiderski RE, Yang B, Carmi R, Stone EM, Sheffield VC (2004) Bbs2-null mice have neurosensory deficits, a defect in social dominance, and retinopathy associated with mislocalization of rhodopsin. *Proc Natl Acad Sci USA* **101:** 16588–16593

Nonaka S, Tanaka Y, Okada Y, Takeda S, Harada A, Kanai Y, Kido M, Hirokawa N (1998) Randomization of left–right asymmetry due to loss of nodal cilia generating leftward flow of extraembryonic fluid in mice lacking KIF3B motor protein. *Cell* **95:** 829–837

Orozco JT, Wedaman KP, Signor D, Brown H, Rose L, Scholey JM (1999) Movement of motor and cargo along cilia. *Nature* **398:** 674

Ou G, Blacque OE, Snow JJ, Leroux MR, Scholey JM (2005) Functional coordination of intraflagellar transport motors. *Nature* **436:** 583–587

Pan X, Ou G, Civelekoglu-Scholey G, Blacque OE, Endres NF, Tao L, Mogilner A, Leroux MR, Vale RD, Scholey JM (2006) Mechanism of transport of IFT particles in *C. elegans* cilia by the concerted action of kinesin-II and OSM-3 motors. *J Cell Biol* **174:** 1035–1045

Pazour GJ, Rosenbaum JL (2002) Intraflagellar transport and cilia-dependent diseases. *Trends Cell Biol* **12:** 551–555

Peden EM, Barr MM (2005) The KLP-6 kinesin is required for male mating behaviors and polycystin localization in *Caenorhabditis elegans*. *Curr Biol* **15:** 394–404

Pedersen LB, Geimer S, Rosenbaum JL (2006) Dissecting the molecular mechanisms of intraflagellar transport in *Chlamydomonas*. *Curr Biol* **16:** 450–459

Perkins LA, Hedgecock EM, Thomson JN, Culotti JG (1986) Mutant sensory cilia in the nematode *Caenorhabditis elegans*. *Dev Biol* **117:** 456–487

Piperno G, Siuda E, Henderson S, Segil M, Vaananen H, Sassaroli M (1998) Distinct mutants of retrograde intraflagellar transport (IFT) share similar morphological and molecular defects. *J Cell Biol* **143:** 1591–1601

Qin H, Burnette DT, Bae YK, Forscher P, Barr MM, Rosenbaum JL (2005) Intraflagellar transport is required for the vectorial movement of TRPV channels in the ciliary membrane. *Curr Biol* **15:** 1695–1699

Reese TS (1965) Olfactory cilia in the frog. *J Cell Biol* **25:** 209–230

Roayaie K, Crump JG, Sagasti A, Bargmann CI (1998) The Ga protein ODR-3 mediates olfactory and nociceptive function and controls cilium morphogenesis in *C. elegans* olfactory neurons. *Neuron* **20:** 55–67

Rohlich P (1975) The sensory cilium of retinal rods is analogous to the transitional zone of motile cilia. *Cell Tissue Res* **161:** 421–430

Rosenbaum JL, Witman GB (2002) Intraflagellar transport. *Nat Rev Mol Cell Biol* **3:** 813–825

Satir P, Christensen ST (2007) Overview of structure and function of mammalian cilia. *Annu Rev Physiol* **69:** 377–400

Schafer JC, Haycraft CJ, Thomas JH, Yoder BK, Swoboda P (2003) XBX-1 encodes a dynein light intermediate chain required for retrograde intraflagellar transport and cilia assembly in *Caenorhabditis elegans*. *Mol Biol Cell* **14:** 2057–2070

Scholey JM (2003) Intraflagellar transport. *Annu Rev Cell Dev Biol* **19:** 423–443

Sengupta P, Chou JH, Bargmann CI (1996) *odr-10* encodes a seven transmembrane domain olfactory receptor required for responses to the odorant diacetyl. *Cell* **84:** 899–909

Signor D, Wedaman KP, Orozco JT, Dwyer ND, Bargmann CI, Rose LS, Scholey JM (1999a) Role of a class DHC1b dynein in retrograde transport of IFT motors and IFT raft particles along cilia, but not dendrites, in chemosensory neurons of living *Caenorhabditis elegans*. *J Cell Biol* **147:** 519–530

Signor D, Wedaman KP, Rose LS, Scholey JM (1999b) Two heteromeric kinesin complexes in chemosensory neurons and sensory cilia of *Caenorhabditis elegans*. *Mol Biol Cell* **10:** 345–360

Singla V, Reiter JF (2006) The primary cilium as the cell's antenna: signaling at a sensory organelle. *Science* **313:** 629–633

Sloboda RD (2005) Intraflagellar transport and the flagellar tip complex. *J Cell Biochem* **94:** 266–272

Snow JJ, Ou G, Gunnarson AL, Walker MR, Zhou HM, Brust-Mascher I, Scholey JM (2004) Two anterograde intraflagellar transport motors cooperate to build sensory cilia on *C. elegans* neurons. *Nat Cell Biol* **6:** 1109–1113

Starich TA, Herman RK, Kari CK, Yeh W-H, Schackwitz WS, Schuyler MW, Collet J, Thomas JH, Riddle DL (1995) Mutations affecting the chemosensory neurons of *Caenorhabditis elegans*. *Genetics* **139:** 171–188

Sulston JE, Schierenberg E, White JG, Thomson JN (1983) The embryonic cell lineage of the nematode *Caenorhabditis elegans*. *Dev Biol* **100:** 64–119

Swoboda P, Adler HT, Thomas JH (2000) The RFX-type transcription factor DAF-19 regulates sensory neuron cilium formation in *C. elegans*. *Mol Cell* **5:** 411–421

Tabish M, Siddiqui ZK, Nishikawa K, Siddiqui SS (1995) Exclusive expression of *C. elegans osm-3* kinesin gene in chemosensory neurons open to the external environment. *J Mol Biol* **247:** 377–389

Takeda S, Yonekawa Y, Tanaka Y, Okada Y, Nonaka S, Hirokawa N (1999) Left–right asymmetry and kinesin superfamily protein KIF3A: new insights in determination of laterality and mesoderm induction by *kif3A−/−* mice analysis. *J Cell Biol* **145:** 825–836

Tichelaar JW, Wert SE, Costa RH, Kimura S, Whitsett JA (1999) HNF-3/forkhead homologue-4 (HFH-4) is expressed in ciliated epithelial cells in the developing mouse lung. *J Histochem Cytochem* **47:** 823–832

Tobin D, Madsen D, Kahn-Kirby A, Peckol E, Moulder G, Barstead R, Maricq A, Bargmann CI (2002) Combinatorial expression of

TRPV channel proteins defines their sensory functions and subcellular localization in *C. elegans* neurons. *Neuron* **35:** 307–318

Troemel ER, Chou JH, Dwyer ND, Colbert HA, Bargmann CI (1995) Divergent seven transmembrane receptors are candidate chemosensory receptors in *C. elegans*. *Cell* **83:** 207–218

Troemel ER, Kimmel BE, Bargmann CI (1997) Reprogramming chemotaxis responses: sensory neurons define olfactory preferences in *C. elegans*. *Cell* **91:** 161–169

Wang Q, Pan J, Snell WJ (2006) Intraflagellar transport particles participate directly in cilium-generated signaling in *Chlamydomonas*. *Cell* **125:** 549–562

Ward S, Thomson N, White JG, Brenner S (1975) Electron microscopical reconstruction of the anterior sensory anatomy of the nematode *Caenorhabditis elegans*. *J Comp Neurol* **160:** 313–337

Ware RW, Clark D, Crossland K, Russell RL (1975) The nerve ring of the nematode *Caenorhabditis elegans*: sensory input and motor output. *J Comp Neur* **162:** 71–110

Young RW, Droz B (1968) The renewal of protein in retinal rods and cones. *J Cell Biol* **39:** 169–184

Yu H, Pretot RF, Burglin TR, Sternberg PW (2003) Distinct roles of transcription factors EGL-46 and DAF-19 in specifying the functionality of a polycystin-expressing sensory neuron necessary for *C. elegans* male vulva location behavior. *Development* **130:** 5217–5227